PARTICLE IDENTIFICATION IN COMPASS RICH 1

Progress Report - September 2001.

P. Schiavon

1 INTRODUCTION

This report is an update of the Progress Report [1], to which I will refer for some details and for comparison of the results.
Further studies on the PID on Likelihood basis are discussed and results on MC events are presented.

2 LIKELIHOOD ANALYSIS

(A) • Likelihood
In this Likelihood estimation, both the signal and the background need to be described correctly. If, as in our case, the theoretical description is not easy, the distributions can be taken from the experimental data (MC data in this study).

As shown in [1], in the θ^{photon}, ϕ^{photon} plane (result of the Rough transformation, relative to a given particle direction, applied to all clusters on the detector planes), the signal can be described quite reasonably, for fixed ϕ^{photon}, by a gaussian distribution $G(\theta^{photon}_{rec,\ k}, \phi^{photon}_{rec,\ k})$ around θ^{ring}_{rec}, with a standard deviation $\sigma^{photon}_{\theta}(\phi^{photon}_{P}, \beta)$.

The background due to the electronics noise of the photon detector (uniformly distributed on the detector surface) can be described by a function $B(\theta^{photon}, \phi^{photon}) \sim \theta^{photon}$, on the Rough plane; for other sources of background, like the Cherenkov photons emitted by the other particles of the same event or recorded because of the memory time of the photon chambers, the description is less evident. As starting point we assume this background as almost uniformly distributed on the detector surface and we try to determine its amount from data.

For each particle mass hypothesis, computing the corresponding Θ^{mass}, given (measured) the particle momentum, the probability density is written as

$$L_N = \prod_{k=1}^{N^{photon}} [\ (1-\epsilon)\ G(\theta^{photon}_{rec,\ k}, \phi^{photon}_{rec,\ k}) + \epsilon\ B(\theta^{photon}_{rec,\ k})\ ]$$

with

$$G(\theta^{photon}_{rec,\ k}, \phi^{photon}_{rec,\ k}) = \frac{1}{\sigma^{photon}_{\theta,\ k}\sqrt{2\pi}}\ \exp(-\frac{1}{2}\frac{(\theta^{photon}_{rec,\ k} - \Theta^{mass})^2}{(\sigma^{photon}_{\theta,\ k})^2}\ )\ \frac{\theta^{photon}_{rec,\ k}}{\Theta^{mass}}$$

$$B(\theta^{photon}_{rec,\ k}) = \frac{2}{(\Theta_M)^2}\ \theta^{photon}_{rec,\ k}$$

both G and B are normalized to unity. ϵ is the background fraction and Θ_M is the upper limit of the θ^{ring}_{rec} range (70. mrad). Note that the radius of the *ring* of a relativistic particle is, in our case, about 182 mm on the detector surface, corresponding to a θ^{ring} of 55.3 mrad.

The Likelihood is then normalized to the number of photons : $L = \sqrt[N]{L_N}$, to compare Likelihood values of different particles.

(B) • Data sample

As already stated, no experimental data being yet available, COMGeant MC events are used.

In particular the present study is done on a sample (IL) of 18000 events, with LEPTO generator (lepto.full p-up.outpipe.fz files), at 100. GeV/c, using the "initial layout" (COMGeant geometry 6.01).

The events are processed by CORAL (the COMPASS reconstruction program) using the TRAFFIC package, for tracking and extrapolating the tracks with a well reconstructed momentum to the RICH entrance window, and the RICHONE code, for RICH reconstruction.

In the RICH hit digitization (MC simulation of the RICH photon chamber behaviour) the background amount (elecronics noise) is given by a 'threshold' set to 2.5; this means roughly that $\simeq$ 1% of the photon chamber pads are activated, uniformly distributed over the detector surface (see fig.s 2 and 14 for an intuitive appreciation).

(C) • Errors assignment

In the Likelihood expression, $\sigma^{photon}_{\theta,\ k}$, the error assumed on the angle θ of each measured photon (regardless it belongs to signal or background), is taken as $\sigma^{photon}_{\theta}(\phi^{photon}_{P,\ k}, \beta)$, depending both on ϕ^{photon}, the azimuthal angle around the particle trajectory, and on the particle β; the suffix P recalls the reference to the 'Particle Plane' (see [1], sec.2, b)).

For practical reasons, at present, the dependence on β is taken into account in the form of a correction:

$\sigma^{photon}_{\theta,\ k} = \sigma^{photon}_{\theta}(\phi^{photon}_{P,\ k})\ \ \sigma^{photon}_{\theta}(\beta)/0.7$.

The parametrizations are :

$\sigma^{photon}_{\theta}(\phi^{photon}_{P}) = \mathrm{C}_0 + \mathrm{C}_1\ cos(\phi_P) + \mathrm{C}_2\ cos(2\phi_P) + \mathrm{C}_3\ cos(3\phi_P) + \mathrm{C}_4\ cos(4\phi_P)$.

$\sigma^{photon}_{\theta}(\beta) = \mathrm{B}_0 + \mathrm{B}_1\ (1.\text{-}\ \beta^2)$, $\qquad \beta = 1/(n_{RI}\ cos\theta^{ring}_{rec})$,

with n_{RI} the refractive index of the radiator gas.

On the event sample IL, they result :

$\mathrm{C}_0 = 0.89$, $\mathrm{C}_1 = 0.0082$, $\mathrm{C}_2 = -\ 0.0516$, $\mathrm{C}_3 = 0.0548$, $\mathrm{C}_4 = 0.0537$.

$\mathrm{B}_0 = 0.795$, $\mathrm{B}_1 = 47.8$.

The factor 0.7 is obtained tuning the shape of the χ^2 distibution of the photons belonging to the reconstructed *ring* (within $\theta^{ring}_{rec} \pm 3\ \sigma^{ring}_{\theta}$) to the expected one (see fig.1 (a)); this value is in good agreement with that obtained optimizing the PID efficiency (see point (E)).

(D) • Background estimation
The background fraction ϵ is defined as $\epsilon = N_B \ / \ (N_S + N_B)$, where N_S is the number of photons in the gaussian peak (signal) and N_B is the number of photons in the background, in the θ_{rec}^{photon} range from 0. to Θ_M (total background).
Assuming a quadratic dependence of the signal on Θ^{mass} (=Θ) of the form $\alpha\Theta^2$ on physical basis, after normalization of the Likelihood, ϵ can be parametrized, at a first approximation, as $1/(\alpha\Theta^2 + 1)$.

In this exercise, α is evaluated from the distribution of θ_{rec}^{photon}, taken in bins of θ_{rec}^{ring} from a data (MC) event sample.
In fig.2 an example of the average distribution of θ_{rec}^{photon} per particle, in 8 bins of θ_{rec}^{ring}, 3 mrad wide, from 52. to 28. mrad, is shown. The fits are to a gaussian shape plus a linear background through 0 of the form : $\alpha\Theta^2 \ G(\theta, \Theta) + B(\theta)$ where $G(\theta, \Theta)$ is the gaussian of the signal and $B(\theta)$ the linear background, as in (A). In such a way α is expected to be constant with Θ.

The shape and the amount of the background under the signal peak is complicated by the presence of the Cherenkov photons emitted by the other particles of the same event (or from the beam halo pile-up) and by the finite acceptance of the detectors. This means that, in the distributions of fig.2, the total amount of background is a function of the angle Θ of the slice considered and the shape of the background is not simply linear with θ_{rec}^{photon}.
The fits to the distributions of fig.2, with a background of variable slope, are not stable. For this reason the background is fitted separately outside the signal peak (see fig.2) to a linear form (first approximation) in θ_{rec}^{photon} and its integral between 0. and Θ_M is parametrized as $B \ (1 + \beta\Theta)$; the value of β obtained is then used in the fit to the distributions of fig.2, assuming the form $\alpha\Theta^2 \ G(\theta, \Theta) + (1 + \beta\Theta) \ B(\theta)$, or correspondingly ϵ parametrized as $(1 + \beta\Theta) \ / \ (\alpha\Theta^2 + 1 + \beta\Theta)$.

Such a description of the background has been reached after processing the MC events in various conditions, like
(a) no electronics noise on photon detectors; the background should be given by the photons of the other particles only;
(b) only one particle (and its Cherenkov photons) per event; this should give no background from the photons of the other particles;
(c) each particle with associated the Cherenkov photons emitted by another particle of the previous event (random association or 'scrambling'); this would simulate an uncorrelated background.
Note that the relevant features of the various tests fit all in a consistent picture, according to what expected; I will not show more details about them.
Moreover, as shown in fig.4, there exists a correlation between θ_{rec}^{ring} ($\sim$ the reconstructed *ring* radius) and the distance of the *ring* centre (on the detector plane) to the origin of the reference (i.e. the point where the optical axis of the corresponding mirror crosses the detector plane). This correlation is because lower momentum ($\sim$ smaller Cherenkov angle) particles are expected to populate more the outer regions of the detectors and we expect less background from other particles for *rings* far from the central region.

In fig.3 the distribution of the parameter α (a) and β (b), as from the fits, in 12 bins of θ_{rec}^{ring}, from 19. to 55. mrad. The fits of the figure are to a constant ($\rightarrow \alpha = 0.00046$) and to a linear form ($\rightarrow \beta = 0.03$); the weights are the errors on the bin contents, the ratio R between the number of photons (N) and the number of corresponding particles (P) ($\sigma_R \simeq R \ / \ \sqrt{P}$).

In fig.5 the same ditributions as in fig.2, but superimposed, to better show the variation of the signal amplitude and of the background slope with Θ; in fig.6 the same ditributions for the case (c) above ('scrambling'): it is of interest to observe how the pattern recognition procedure, in the presence of a significant background, is forced to find in any case a *ring* of random radius with an average number of photons, function of the background density, ≤ 4 in this exercise; as an obvious consequence, a lower limit for the number of photons per *ring* to be accepted is necessary (at present set to 5).

As a consistency check, in fig.7 (a) the total number of photons per particle is plotted as a function of Θ of the slice for the bins used in the fitting procedure above, together with the total background as from the fits; in (b) the signal obtained both as difference of the two distributions in (a) and from the peak area from the fits above; the agreement between the two distributions is quite good; the line is a fit to a form $A(1 + \alpha\Theta^2)$ which leeds to a value of α ($\rightarrow 0.00042$) in good agreement with the value above; moreover the value of A (3.0) is in agreement with the conclusions of fig.6.

As a further consistency check, a similar approach has been used, looking at the distribution of $\theta_{rec}^{photon} - \theta_{rec}^{ring}$ again in bins of θ_{rec}^{ring} ; see fig.8. In this case too a fit has been performed to a form of a gaussian peak plus a linear background; fig.9 (a) shows the background under the signal, in the $\pm 3 \ \sigma_{\theta}^{photon}$ region, as a function of Θ, (b) the extrapolated total background; the line is a weighted fit to a form $B(1 + \beta\Theta)$, giving a value of β of 0.028 and (c) the signal distribution from which a value of α of 0.00046 is obtained, both in very good agreement with the previous values.

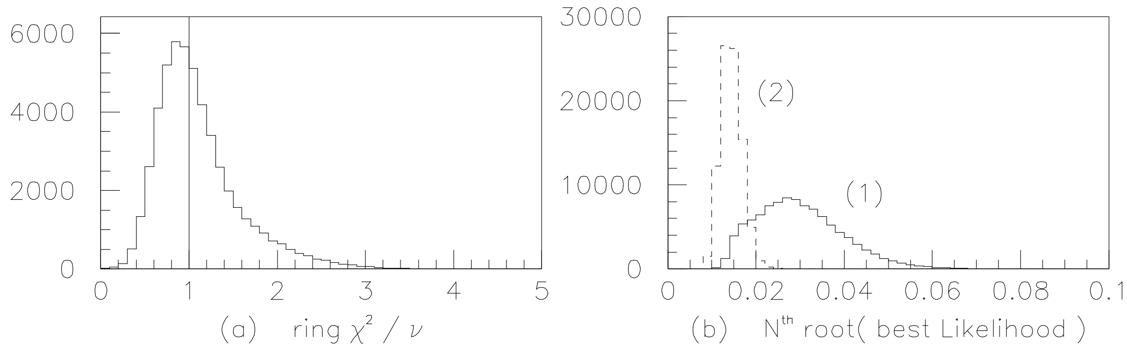

Figure 1: (a) The distibution of the χ^2 of the reconstructed *ring*, normalized to the number of degrees of freedom ν, after the tuning of the errors. (b) The distribution of the best Likelihood (1), normalized ($\sqrt[N]{L}$) to the number of photons N and the distribution (2) of the best Likelihood when processing 'scrambled' particles and pads, i.e. pure background.

(E) • PID results

For each particle with a reconstructed *ring*, the likelihood L is evaluated for three mass hypotheses, π, K and p, being the lower masses undistinguishable from pions. The mass

hypothesis with the largest L value is taken as the good one.
In the present approach, for the evaluation of L, we use all the 'photons' with, after the Rough transformation, a θ_{rec}^{photon} smaller than 70. mrad; this is different from the approach of the previous report ([1]) where in the computation of the χ^2 or of the L were used only the photons belonging to the reconstructed *ring* (within $\theta_{rec}^{ring} \pm 3\ \sigma_{\theta}^{ring}$).
In fig.1 (b) the distribution of the largest Likelihood value, (1), normalized ($^{N}\sqrt{L}$) to the number of 'photons', is shown. Note that the average value is about one order of magnitude smaller than that of the exercise in [1] because of the larger number of background 'photons'.
The distribution (2) is that of the largest Likelihood value when processing 'scrambled' particles and pads, i.e pure background *rings*; it is worth to note that there is no full separation between the two distributions; the suggestion of putting a lower limit to the L value is to be handled very carefully.

In table 1 the results of the Likelihood particle mass assignments are shown. The sum of each column corresponds to the number of particles, of the type indicated, generated in the MC simulation and accepted for identification, and each entry of the column is the number of particles of the type identified by the Likelihood according to the label of the row. Along the diagonal we then get the identification efficiencies (number of particles correctly identified over accepted for ID), i.e. 99.8 % for $\pi's$, 99.0 % for $K's$ and 99.1 % for $p's$, whereas looking at the rows, we get the sample contamination (number of wrong identifications over number of particle identified for the given mass), i.e. $\simeq$ 0. % for $\pi's$, 2.9 % for $K's$ and 3.9 % for $p's$.
Varying the error correction factor (point (C)) we get small changes in the percentages, confirming its value of point (C).
Note that the totals of the columns are the particles which are accepted for the identification; due to the reconstruction cuts (small deflection inside the RICH of the incoming particle, particle momentum over the Cherenkov threshold, number of photons in the reconstructed *ring* over a minimum (set to 5), ...) they result to be respectively the 94.3 % for $\pi's$, 89.6 % for $K's$ and 85. % for $p's$ of the particles input to the RICH.

Table 1 should not be compared with the corresponding table of [1] because of many different conditions (more realistic COMGeant simulation, tracking with TRAFFIC, more noise on chambers, different statistics...). Table 3 gives instead the corresponding results using the Likelihood procedure of [1] in the present context: the identification efficiency is 99.9 % for $\pi's$, 98.6 % for $K's$ and 96.5 % for $p's$) and the sample contamination 0.1 % for $\pi's$, 2.1 % for $K's$ and 2.3 % for $p's$. The comparison points out that, with the present Likelihood, we have a moderate gain in the identification efficiency together with a sligthly larger sample contamination.

In fig.10 the efficiency of particle identification is shown as a function of the momentum, in (a) for $\pi's$, in (b) for $K's$ and in (c) for $p's$.
In fig.11 the efficiency of particle identification as a function of the number of photons in the reconstructed *ring* (no background subtraction);
The fig.12 shows the mass spectrum of the particles as identified, for all momenta, split into the mass region of the π (a), of the K (b) and of the p (c).

Let stress that, in a previous simpler approach, equivalent to setting to 0. the β

parameter (i.e. neglecting the dependence on Θ of the background slope), with a different value of the parameter α as given by the corresponding fits ($\alpha \simeq 0.00025$), we get comparable good results (see table 2). It can be outlined that the quality of the results is really equivalent, within the statistical limits, and, on the other hand, from the comparison of tables 1 and 2 and 3 too, that the entries of the tables over the diagonal grow together whereas those under the diagonal diminish, or vice versa; this means that if a background description enhances the PID efficiencies, it enhances too the contaminations. This effect is connected with the Likelihood slope, as discussed in point (F) below and shown in fig.13.

id p	15	7	545
id K	54	1876	3
id π	29042	12	2
	gen π	gen K	gen p

Table 1: Likelihood particle mass assignments for π, K and p.

id p	20	9	547
id K	66	1875	2
id π	29025	11	1
	gen π	gen K	gen p

Table 2: Likelihood particle mass assignments for π, K and p; simplified background description.

id p	11	2	551
id K	30	1884	10
id π	29409	25	10
	gen π	gen K	gen p

Table 3: The particle mass assignments for π, K and p using the Likelihood procedure of report [1].

Instead of the value of L, the Likelihood ratio $R = L \ / \ L_{MAX}$ has been used with no improvement in the PID efficiency (even slightly worse); we can expect that because the Likelihood ratio resolution $dR/R = \sqrt{dL(\Theta^{mass})/L(\Theta^{mass}) + dL(\theta_{MAX})/L(\theta_{MAX})} \geq dL(\Theta^{mass})/L(\Theta^{mass})$; θ_{MAX} is the value of Θ^{mass} at which L has the maximum value L_{MAX}.

(F) • Likelihood shape
To a better undertanding, the Likelihood function has been studied in some details.
For a given particle, the shape of the Likelihood has been plotted for Θ^{mass} varying continuously from 0. to Θ_M; fig.13 shows in (a), (b) and (c) the Likelihood shape for three identified pions with momenta as indicated in the figures; the vertical lines indicate the positions of the expected value of the *ring* angle, given the particle momentum, for each particle mass; it is evident as at higher momenta the PID power becomes smaller.
It is also interesting to note, for a given amount of background, the decreasing shape of the Likelihood due to the signal to noise ratio as a function of θ^{ring}, as discussed in (D), and to the Likelihood normalization; as a less evident consequence, see fig.13 (c), the Likelihood value for the proton hypothesis can be larger than that of the kaon, even if the kaon *ring* radius is closer to that of the identified pion.
The lines are $L_{N,B}(\Theta)$, the background contribution to L, i.e., with reference to the expressions of points (A) and (D), ($N = N^{photon}$),

$$L_{N,B}(\Theta) = \prod_{k=1}^{N} \epsilon \ B(\theta^{photon}_{rec,\ k}) \ = \ [\ (1+\beta\Theta)/(\alpha\Theta^2+1+\beta\Theta) \ \ 2/\Theta_M^2\ ]^N \prod_{k=1}^{N} \theta^{photon}_{rec,\ k}$$

The fig.14 (right) shows the same for an identified proton, together with a display of its *ring* (left); under the Likelihood shape, the distribution of the reconstructed 'photons' from which the signal peak (*ring*) is extracted. Note the clusters along the *ring* and the background; the circles drawn (left) and the lines drawn (right) correspond to the three mass hypotheses; the square lines are the photon chamber limits.

Tests have been done using a Likelihood in which the background shape $L_{N,B}(\Theta)$ has been subtracted, after normalization ($\sqrt[N]{L_{N,B}}$), from L; see the fig.15 for an exemple; the resulting Likelihood ID power is even a bit worse, much like for the Likelihood ratio R of point (E).

After identification, a good monitor of the reconstruction resolution is given by the distribution of the difference between θ^{ring}_{rec} ($= \theta_{MAX}$ of point (E)) and Θ^{mass}_{ID}; fig,16 shows this distribution for relativistic particles; the standard deviation of a fit to a gaussian form in the peak region is given.

3 EVENT SAMPLE ON THE 2001 LAYOUT

A preliminary analisys has been done on a sample (01) of MC events based on the (still provisional and possibly redundant) layout for the run 2001, at 160. Gev/c, (COMGeant geometry 6.06).
Table 4 is the same as table 1; the corresponding PID efficiencies go down to 99.1 % for $\pi's$, 98.0 % for $K's$ and 97.5 % for $p's$, whereas the wrong identifications grow to $\simeq$ 0.1 % for $\pi's$, 8.9 % for $K's$ and 10.6 % for $p's$; this worsening is in some way expected as an effect of the smaller track reconstruction precision due mainly to the limited number

of tracking detectors and also because the efficiencies are averaged over a larger particle momentum range, due to the higher beam momentum; but we have also to stress that no tuning of the RICHONE methods on the 01 sample has been done yet in this analysis.
In fig,17 the PID efficiencies versus the particle momentum; the statistics limits the comparison of the PID power with respect to fig.10, but the larger momentum range shows clearly the decreasing PID efficiency at higher momenta.

	gen π	gen K	gen p
id p	77	12	751
id K	247	2649	12
id π	34210	41	7

Table 4: Likelihood prticle mass assignments for π, K and p for the (provisional) layout of the run 2001.

4 CONCLUSIONS

A full revision of the PID procedure has been carried out. A modified Likelihood function gives some moderate improvements in the RICH mass identification power and, more important, a better understanding of the general picture has been obtained.

References

[1] P. Schiavon, “Particle Identification in COMPASS RICH1, Progress Report, May 2000; on COMPASS Web

[2] P. Schiavon, “Trieste reconstruction software for COMPASS RICH 1”, December 1999; on COMPASS Web

[3] P. Schiavon, “Studies of the Cherenkov emission angle reconstruction”, Part 1, June 1997; on COMPASS Web

[4] P. Schiavon, “Studies of the Cherenkov emission angle reconstruction”, Part 2, October 1997; on COMPASS Web

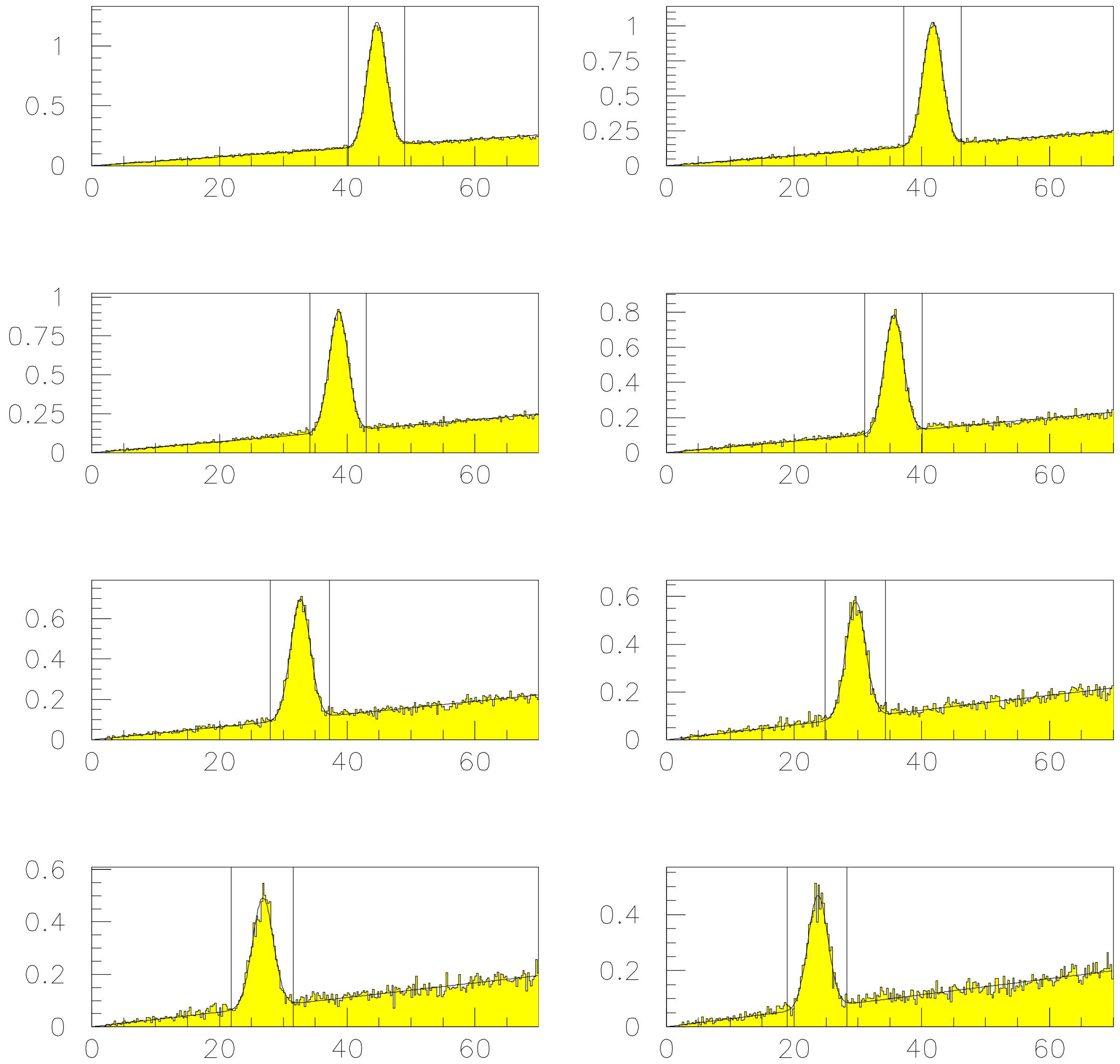

Figure 2: An example of the distribution of θ_{rec}^{photon} (mrad), normalized to one particle, in 8 bins of θ_{rec}^{ring}, 3 mrad wide, from 52. to 28. mrad. The fits are to a gaussian shape plus a linear background through 0. The vertical lines show the $\pm 3\ \sigma_{\theta}^{photon}$ region around the peak.

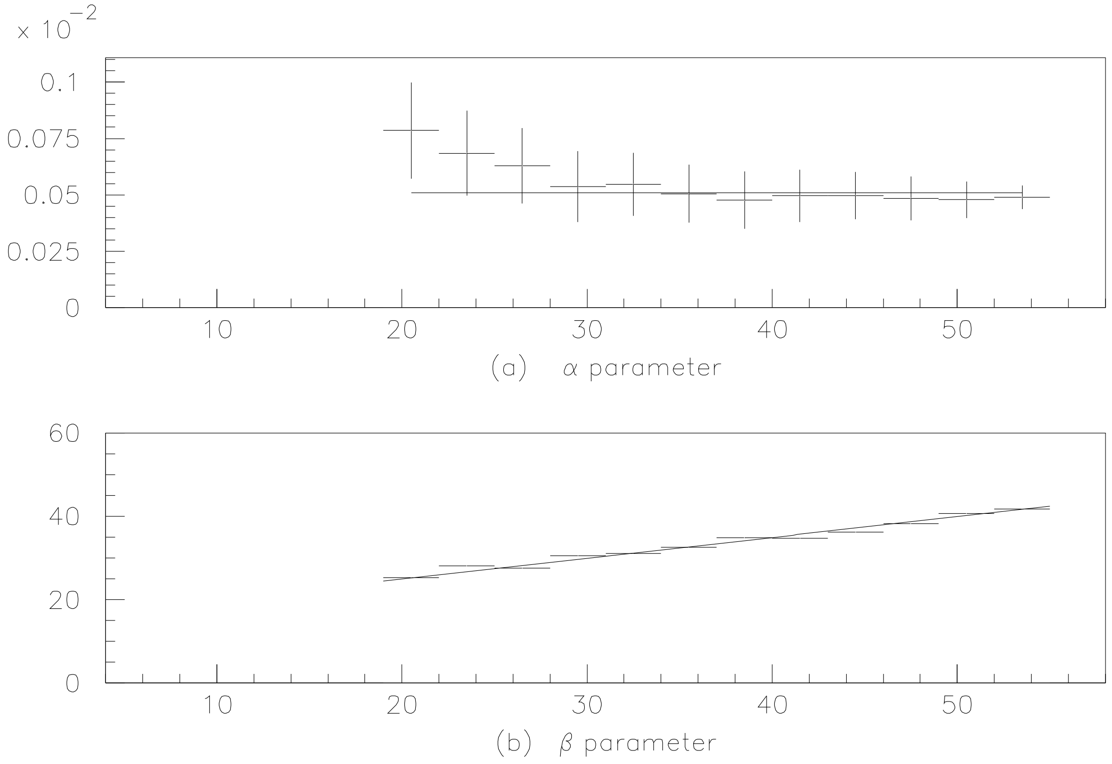

Figure 3: The figure shows in (a) the distribution of the background parameter α as a function of Θ (mrad); in (b) the background parameter β; the weighted fits are to a constant and to a linear form (see the text for details). The histograms are normalized to one particle.

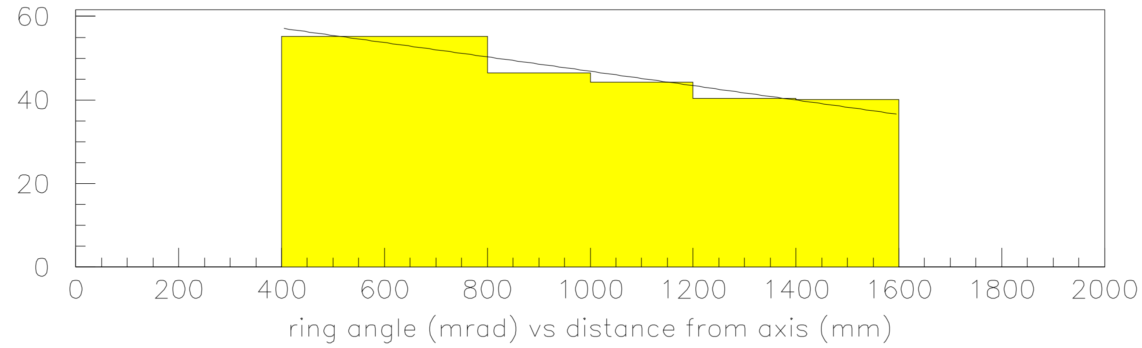

Figure 4: The (almost linear) correlation between the recontructed *ring* angle ($\sim$ radius) (mrad) and the radial distance of its centre.

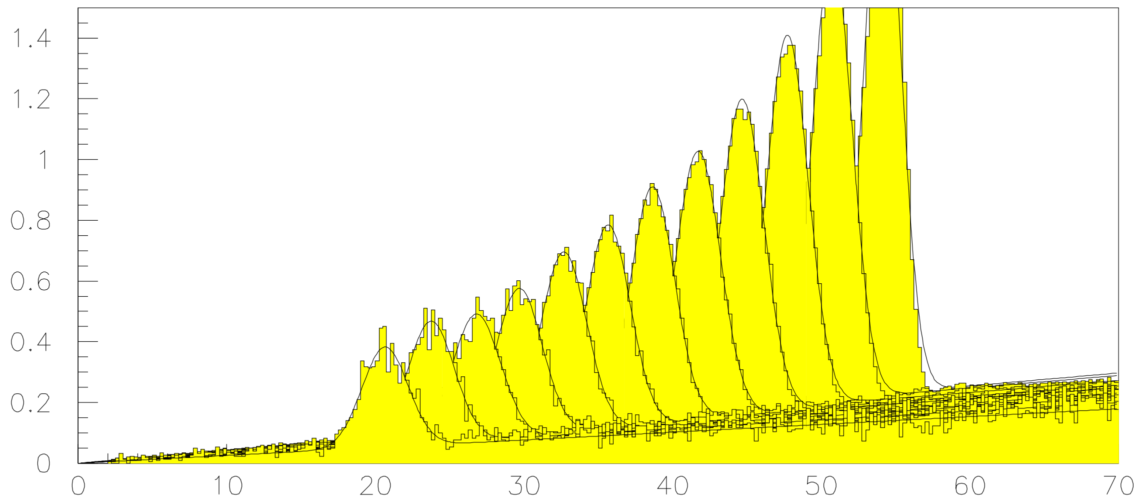

Figure 5: The distributions of signal and background, as a function of θ_{rec}^{photon} (mrad), normalized to one particle, for the different bins of Θ, plotted superimposed to show the variation of the signal amplitude and of the background slope with Θ.

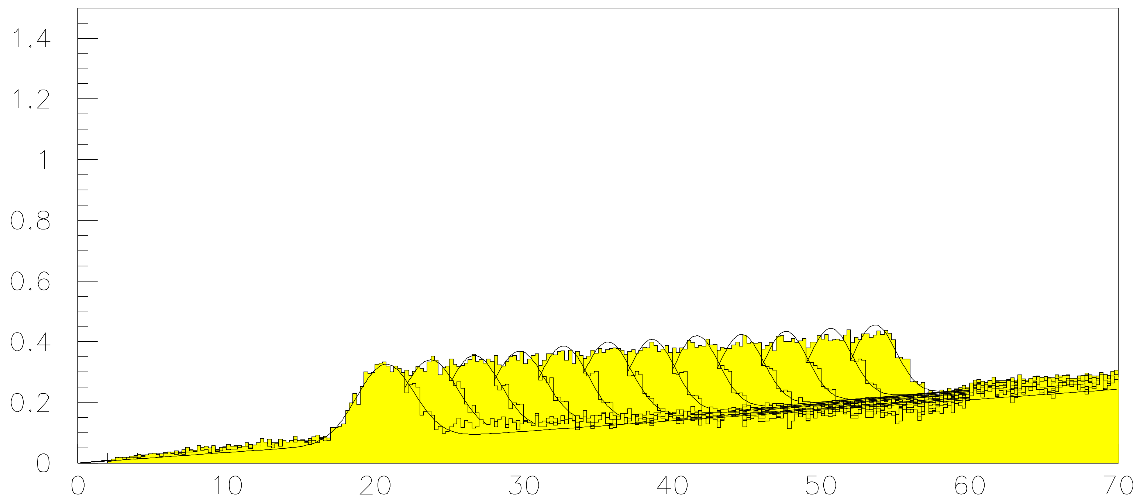

Figure 6: The same distributions of fig.5 but for 'scrambled' processing (see the text); the signal amplitude is constant, as well as the background slope.

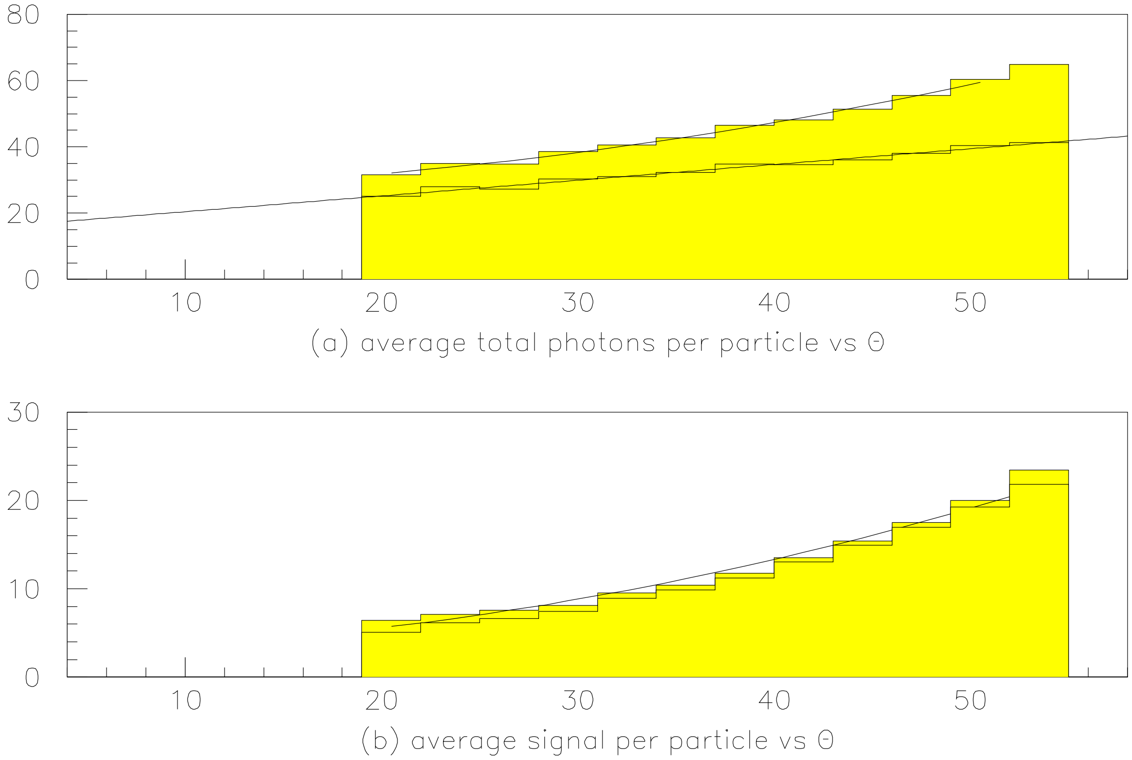

Figure 7: (a) The total number of photons per particle as a function of Θ for the bins used in the fitting procedure described in the text, together with the total background as from the fits; in (b) the signal obtained both as difference of the two distributions in (a) and from the peak area from the fits; the agreement between the two distributions is quite good;

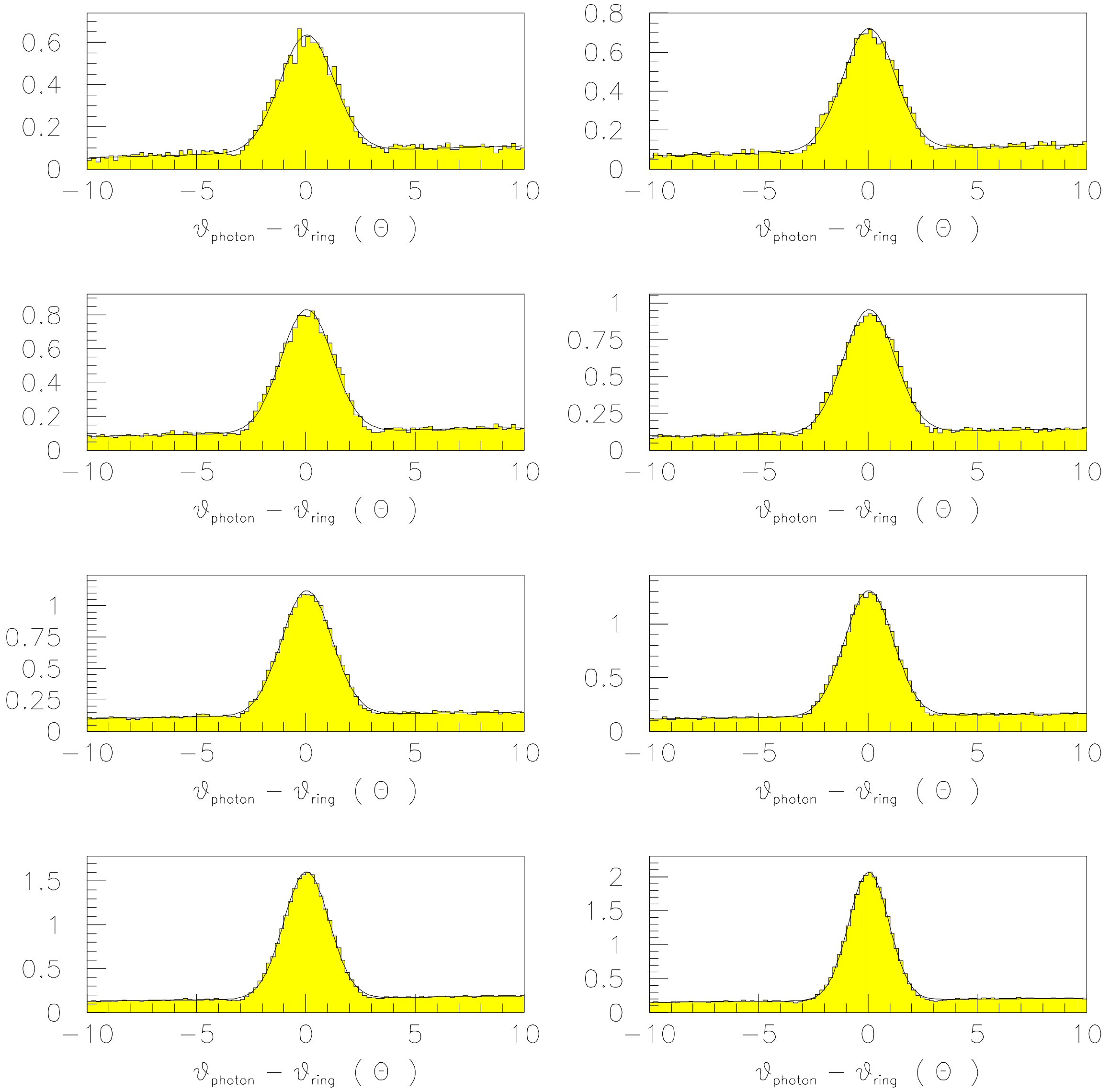

Figure 8: The distribution of $\theta_{rec}^{photon} - \theta_{rec}^{ring}$ (mrad) in the same bins of θ_{rec}^{ring} as in fig.2; the fits are to a gaussian peak plus a linear background.

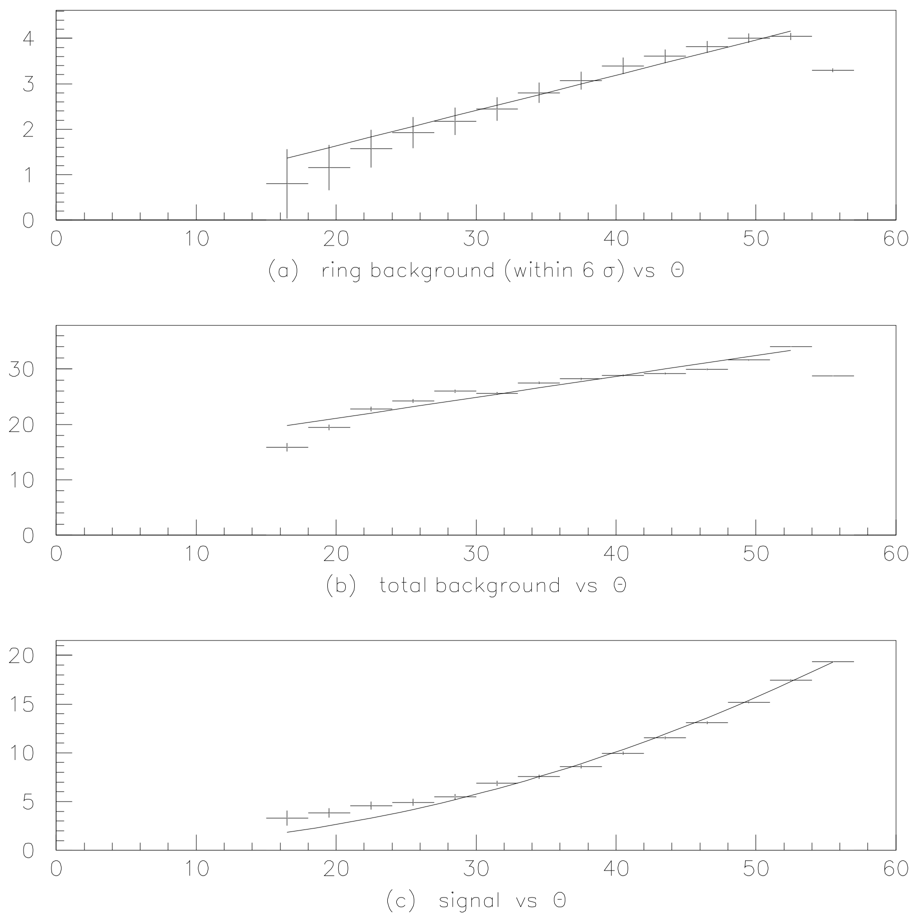

Figure 9: (a) shows the background under the signal, in the $\pm 3\ \sigma_{\theta}^{photon}$ region, as a function of Θ, (b) the extrapolated total background and (c) the signal distribution; from them values of the parameters α and β are obtained in very good agreement with the previous ones; the lines are weighted fits.

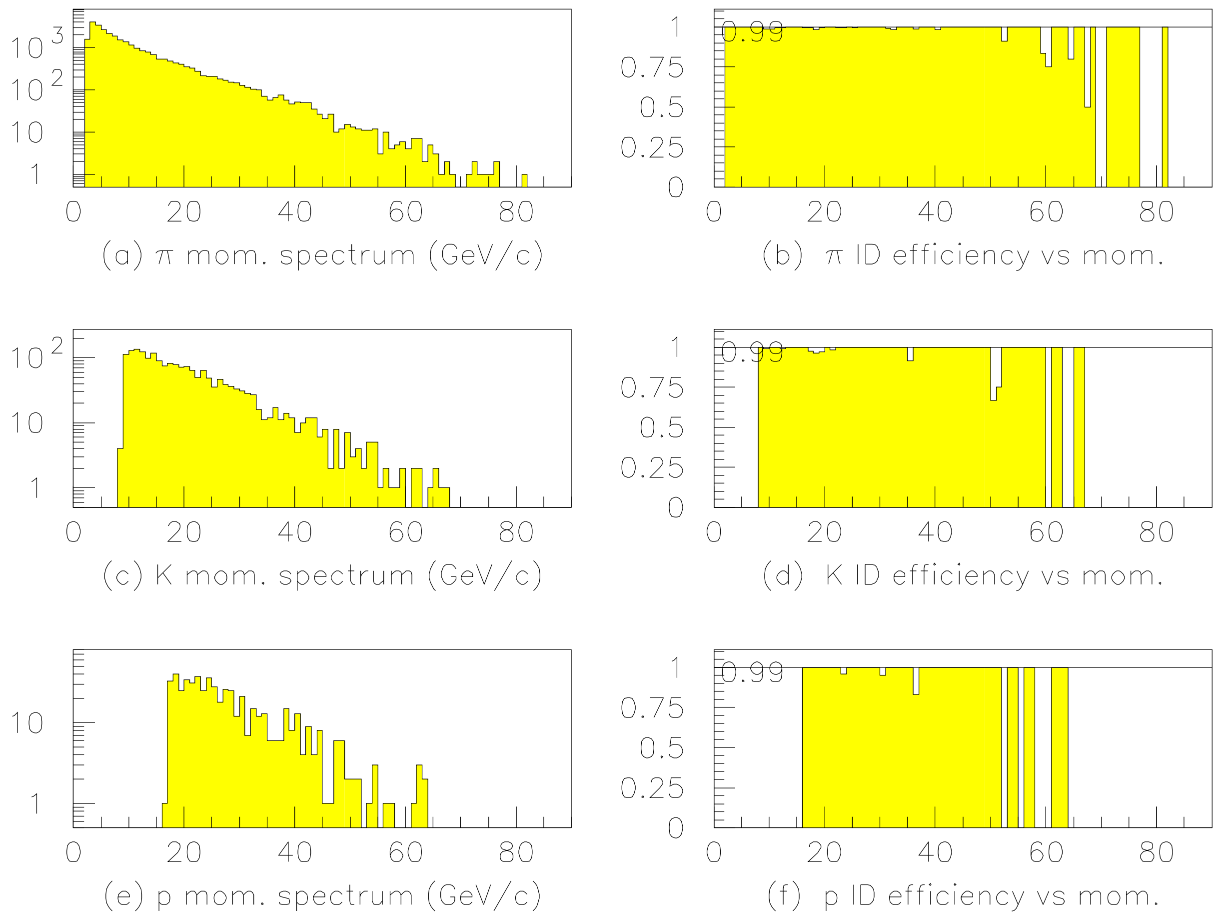

Figure 10: The momentum spectrum and the identification efficiency of the Likelihood method, using the MC information, as a function of the particle momentum, for $\pi's$ (a) and (b), $K's$ (c) and (d) and $p's$ (e) and (f).

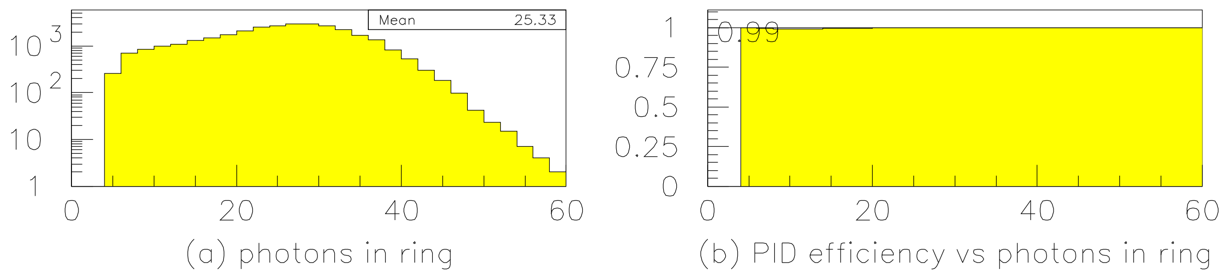

Figure 11: The photon spectrum of the reconstructed *ring* (a) and the identification efficiency (b) as a function of the number of photons in the *ring*.

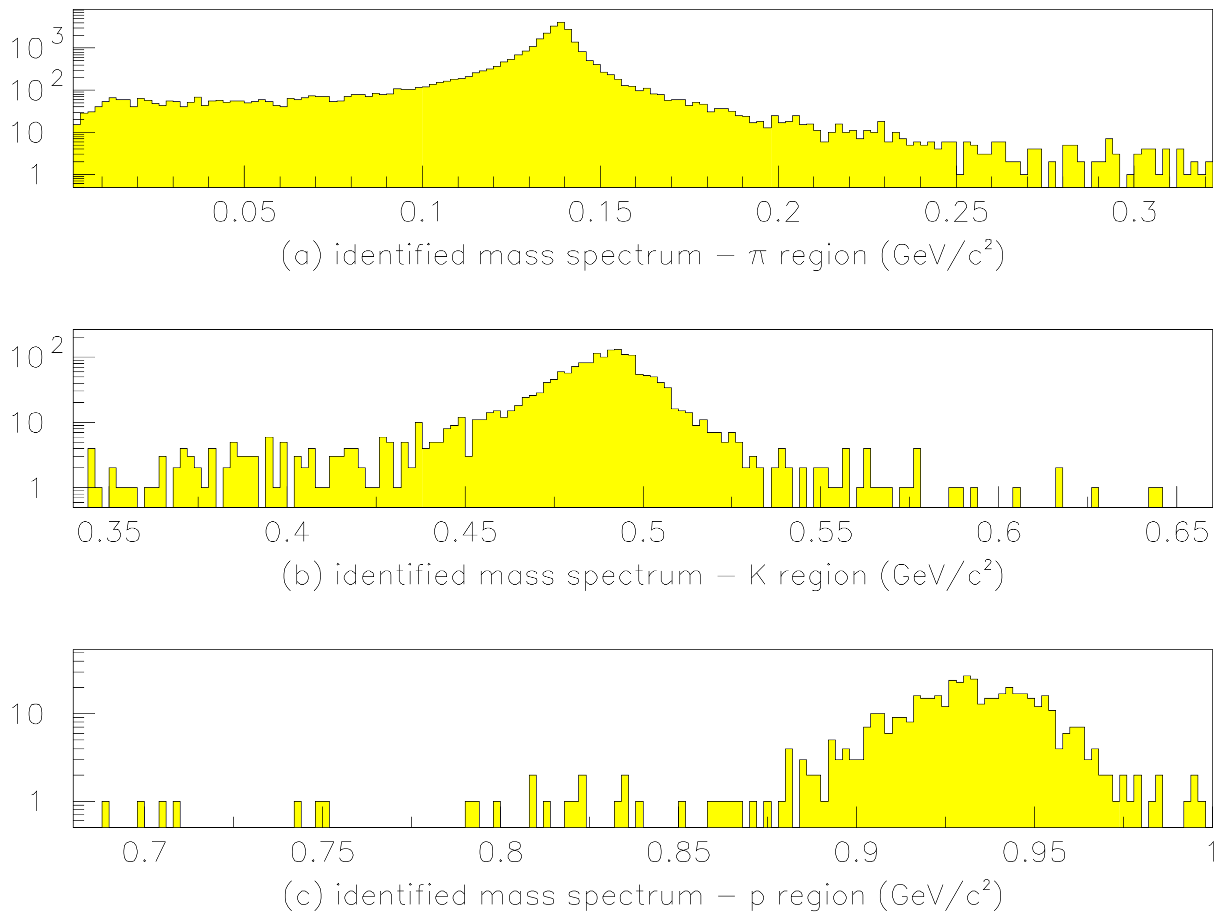

Figure 12: The mass spectrum of the identified particles in the mass region of the π(a), of the K (b) and of the p (c).

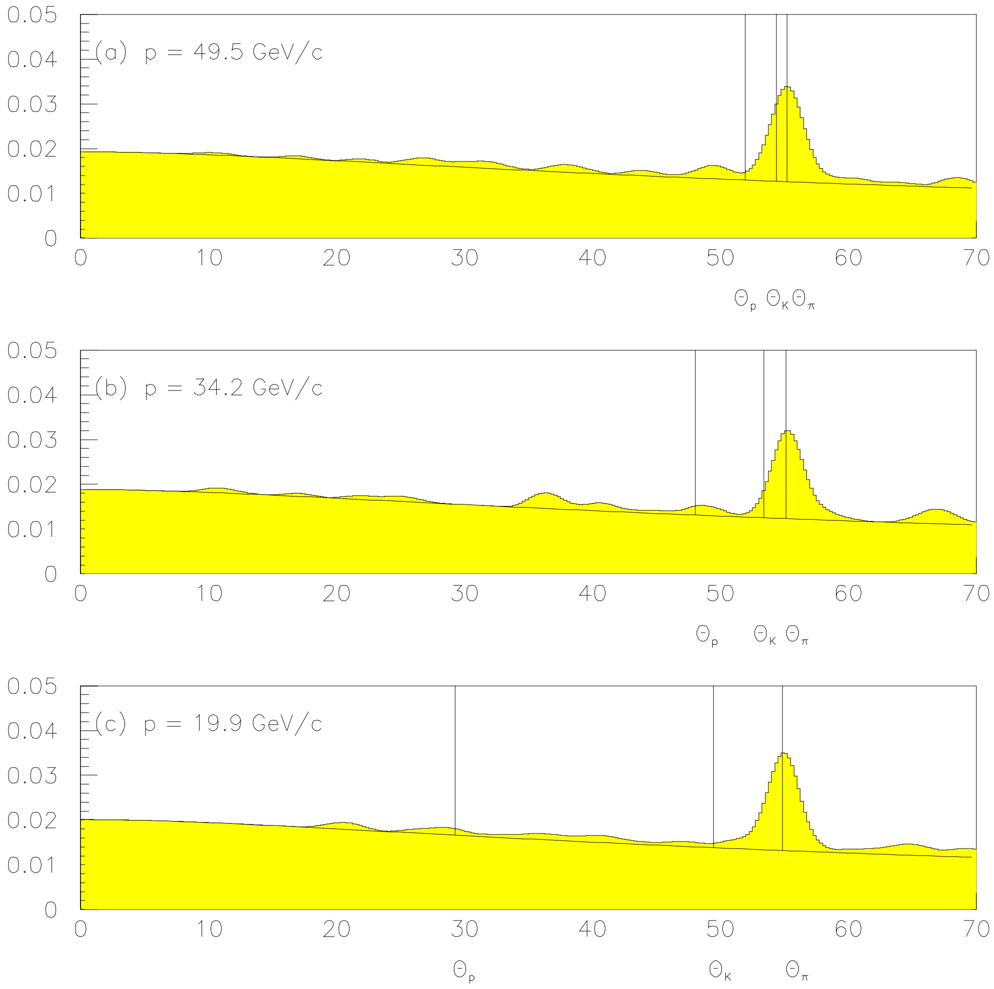

Figure 13: The Likelihood shape as a function of Θ^{mass} (mrad) for three identified pions with momenta as indicated in the figures (a), (b) and (c); the vertical lines indicate the positions of the expected value of the *ring* angle, given the particle momentum, for each particle type; it is evident as at higher momenta the PID power becomes less and less. The curves show the background contribution $L_{N,B}(\Theta)$ (see the text) to the Likelihood.

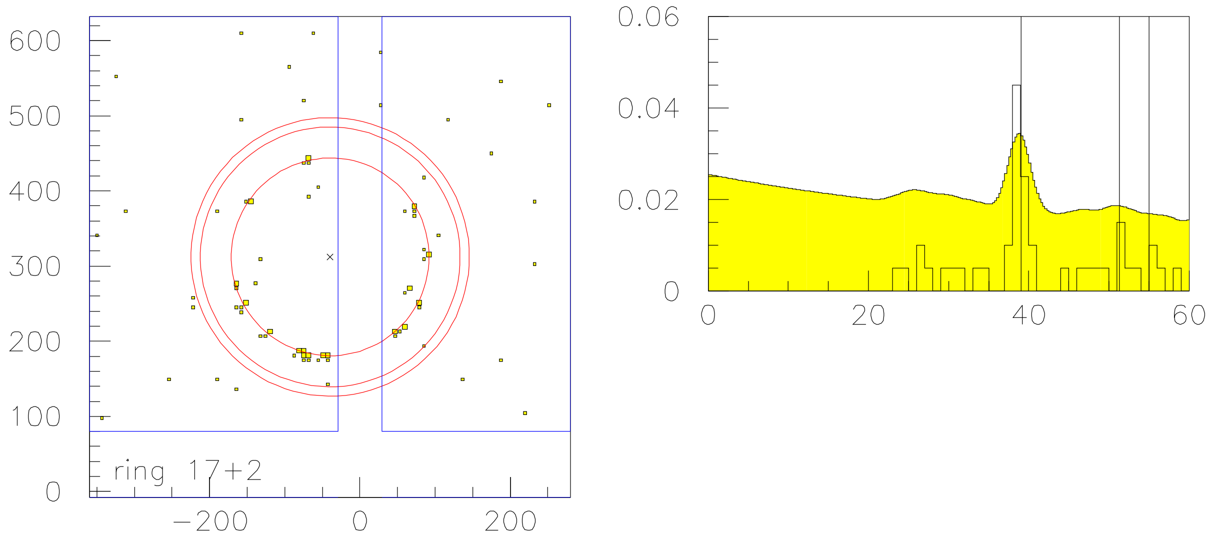

Figure 14: The figure shows (right) the Likelihood shape for an identified proton with superimposed the distribution of the reconstructed 'photons' (not to scale) from which the signal peak (*ring*) is extracted.; a display of its *ring* is also given (left); the different mass hypotheses are drawn as circles (left) or lines (right).

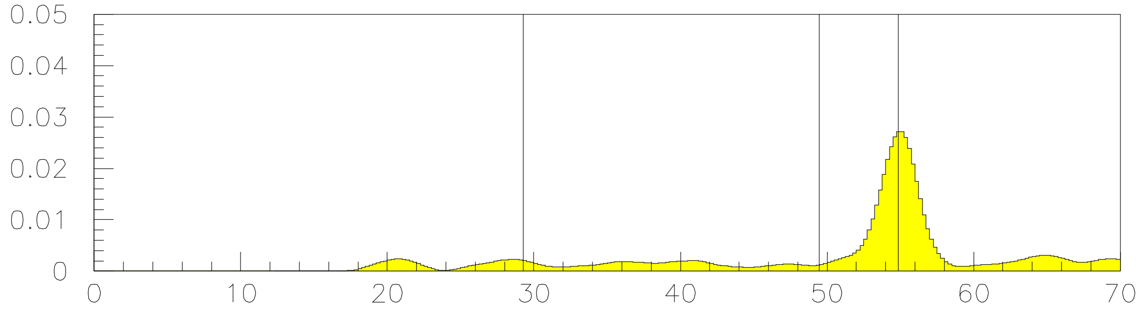

Figure 15: The Likelihood shape as a function of Θ^{mass} (mrad), after the background subtraction.

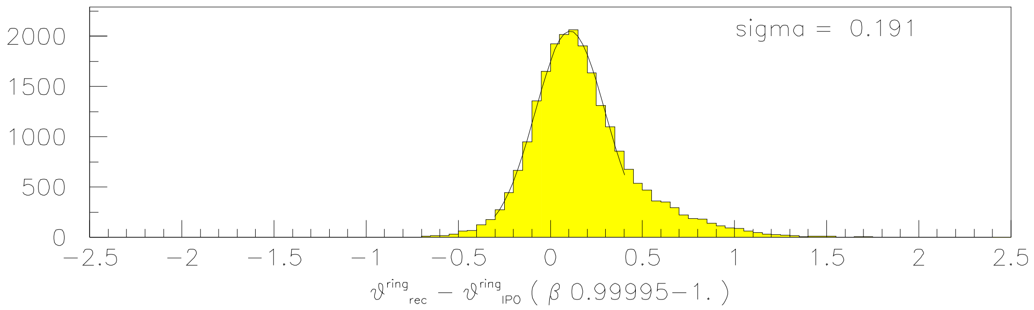

Figure 16: The reconstruction resolution, as the disribution of θ_{rec}^{ring} - Θ_{ID}^{mass} (mrad).

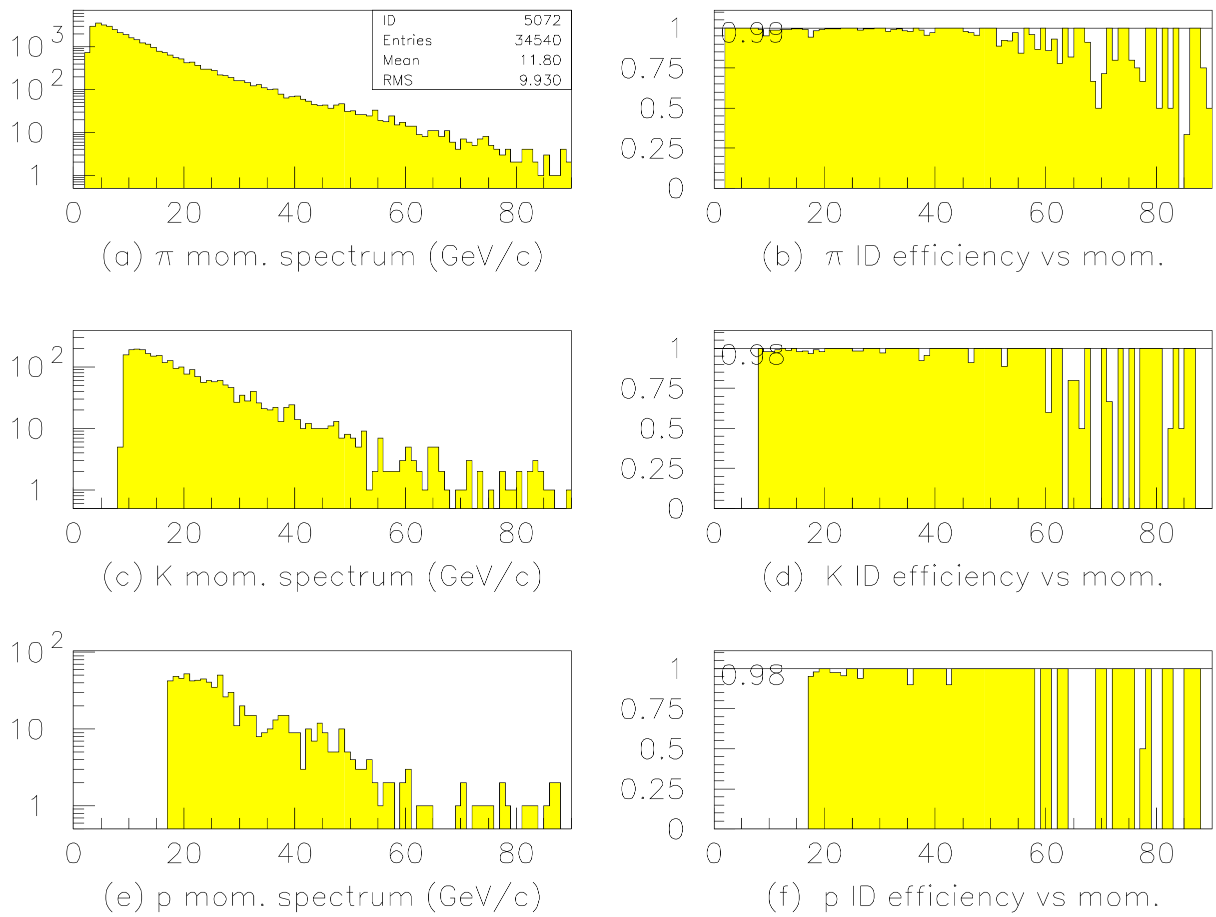

Figure 17: The momentum spectrum and the identification efficiency of the Likelihood method, using the MC information, as a function of the particle momentum, for $\pi's$ (a) and (b), $K's$ (c) and (d) and $p's$ (e) and (f), for the (provisional) layout of the run 2001.